8-2020

Thermal Modeling and Analysis of Roadway Embedded Wireless Power Transfer Modules

Arden N. Barnes
Utah State University

THERMAL MODELING AND ANALYSIS OF ROADWAY EMBEDDED WIRELESS POWER TRANSFER MODULES

by

Arden N. Barnes

A thesis submitted in partial fulfillment
of the requirements for the degree

of

MASTER OF SCIENCE

in

Mechanical Engineering

Approved:

Nicholas Roberts, Ph.D. Major Professor	Hailei Wang, Ph.D. Committee Member
Abhilash Kamineni, Ph.D. Committee Member	Richard S. Inouye, Ph.D. Vice Provost for Graduate Studies

UTAH STATE UNIVERSITY
Logan, Utah

2020

ABSTRACT

Thermal Modeling and Analysis of Roadway Embedded Wireless Power Transfer Modules

by

Arden N. Barnes, Master of Science

Utah State University, 2020

Major Professor: Nicholas Roberts, Ph.D.
Department: Mechanical and Aerospace Engineering

Wireless charging of electric vehicles is a developing technology which potentially increases efficiency and safety. In addition, wireless charging allows for dynamic charging of vehicles by use of smart autonomous roadways. Such roadways would require charging coils to be embedded in concrete, which is thermally insulating, and therefore poses problems to placing heat sensitive components into it. Although the electrical aspects of embedded wireless charging coils have been explored, the thermal aspects have not been explored in depth. This thesis seeks to better understand the thermal behavior of induction coils embedded in a roadway. This is accomplished by performing experiments to determine certain thermal properties of materials used in roadways and inductive charging coils and using those properties in computer models of actual induction coils embedded in concrete. Specifically, the thermal conductivity of concrete is determined by creating a cylindrical system with a heater in the middle and concrete surrounding it then measuring key temperatures at steady-state and comparing to a computer model of the system in ANSYS Fluent. The thermal behavior of an embedded coil is determined in a similar manner; by creating a model of the existing embedded coils and comparing the simulated behavior with the measured behavior at key measurement points. The model will help determine any necessary duty cycle limitations to prevent overheating of the charging coil components

as well as help determine optimal charging patterns for heat dissipation. The benefit of including a phase change material to encase heat generating components of the charging coils is also analyzed by constructing a concrete pad and corresponding model with phase change material included and comparing the thermal behavior to that of a pad and model without any phase change material included. The inclusion of phase change material should increase the thermal response time of the system and allow it to run for longer periods of time without overheating.

(51 pages)

PUBLIC ABSTRACT

Thermal Modeling and Analysis of Roadway Embedded Wireless Power Transfer Modules

Arden N. Barnes

Wireless charging of electric vehicles is a developing technology which potentially increases efficiency and safety. It also allows for charging vehicles while they are moving by having charging stations embedded in the roadway. Because roadways are thermally insulating, it is important to know how the heat from the charging stations will move through the roadway, which will allow further research into whether the heat will cause damage to the components in the station or to the roadway. This thesis studies the way the heat moves through concrete with wireless charging coils embedded in it. This is accomplished by measuring the relevant material properties of materials used in such a system of concrete and charging components and using those properties in a simulation. Specifically, to measure the properties of concrete, an experiment with a matching computer simulation is used. These measured properties and others are then used in a different computer simulation to explore how quickly a charging station will heat up. This simulation is compared to experiments on a real charging station for validation. A station with a material designed to absorb heat implemented is also compared to a station without such a material in an effort to understand other ways of managing the heat generation within the station.

ACKNOWLEDGMENTS

I would like to thank the following people: My advisor, Dr. Nick Roberts, for helping me understand how my contributions can still be valuable even if I think they're incomplete. Amir Behbahanian for running the stepped-bar apparatus. Benny Varghese for making the electrical side of this actually happen. John Mermigas for putting the concrete forms together and all the other miscellaneous things he helped with.

Arden N. Barnes

CONTENTS

LIST OF TABLES

LIST OF FIGURES

ACRONYMS

EV	electric vehicle
FAC	fly ash concrete
HSC	high strength concrete
NSC	normal strength concrete
PCM	phase change material
SCC	self-consolidating concrete
WPT	wireless power transfer

CHAPTER 1

INTRODUCTION

1.1 Motivation

With the increasing popularity of electric vehicles comes an increasing need for charging infrastructure for those vehicles. Currently, the most popular method is plug-in charging, which has an efficiency of 86% [1]. Although such efficiency is good, it has been reported that efficiency of at least 90% is attainable using wireless power transfer (WPT) [2–4] in high power applications such as charging electric vehicles. Although 4% is not a very large number, for such high power applications, efficiency improvements can result in considerable savings in power demand and, consequently, cost. In addition, any energy lost typically becomes heat, which at high power levels can result in degraded performance and in extreme cases, damage to the system. Such high heat and power can also be a safety concern.

In addition to the possibility of greater efficiency, WPT also allows for dynamic charging of electric vehicles via smart autonomous roadways. A smart autonomous roadway is a powered roadway which has the ability to communicate with vehicles and has sensing and charging infrastructure embedded into it [5]. A vehicle traveling on such a roadway could communicate its position and the road would energize the charging coils just as the vehicle passed over them [2, 3, 6]. This means that vehicles can be charged while moving, which can increase the range of electric vehicles and thus reduce range anxiety [4], which is a significant barrier to adopting electric vehicles. Other benefits of WPT are added safety and convenience. Coils embedded in the same fashion in a parking are would be able to charge vehicles without the hassle of plugging them in. Wireless charging also lessens the risk of electric shock by eliminating exposed wires.

Although the concepts have been proven in some way or another, a major barrier to implementing high power charging in roadways is adequate thermal management of the

components. Previous studies on WPT systems embedded in concrete have shown that embedding does not prevent induction from working. Dynamic charging has also been demonstrated [2, 6, 7] but the thermal aspects of these projects are not covered in detail. While there have been efforts to understand the thermal aspects of such a system [8, 9], these steps are only preliminary to understanding what will be required to embed high powered WPT systems in concrete.

To better understand the thermal state of a fully embedded system, it is necessary to know the thermal properties of the material the system is embedded in. Concrete is a composite material, and thus certain methods of determining thermal conductivity and heat capacity cannot be used. Some models have been developed to predict thermal conductivity based on porosity and density [10–12], but determining porosity can be difficult, and the results can have up to a 14% error [12]. There are simpler models based only on density and water content [13] as well. However, due to the many different varieties and mixtures of concrete and cement that exist, any model is impossible to use without first verifying that the model is valid for the concrete being studied or used.

This document outlines what will be required for high powered WPT systems to be embedded in concrete. Since an accurate thermal model requires accurate material properties, attention is given to determining thermal properties of concrete. A computer model with estimated heat generation is then used to explore different methods of thermal management. The computer model will then be validated using physical experiments.

1.2 Literature Review

Currently, the only way to increase the range of an electric vehicle is to increase the capacity of the battery on board. Without major innovation in chemical battery technology, the only method of increasing battery capacity is to increase battery mass and volume. This is not an ideal solution since batteries are costly and the bigger the battery that's carried, the more energy needs to be used to move the vehicle. This trend is shown in Figure 1.1. There are no electric vehicles with high battery weights that do not consume more energy per kilometer traveled. In addition, thermal management of large batteries is difficult and

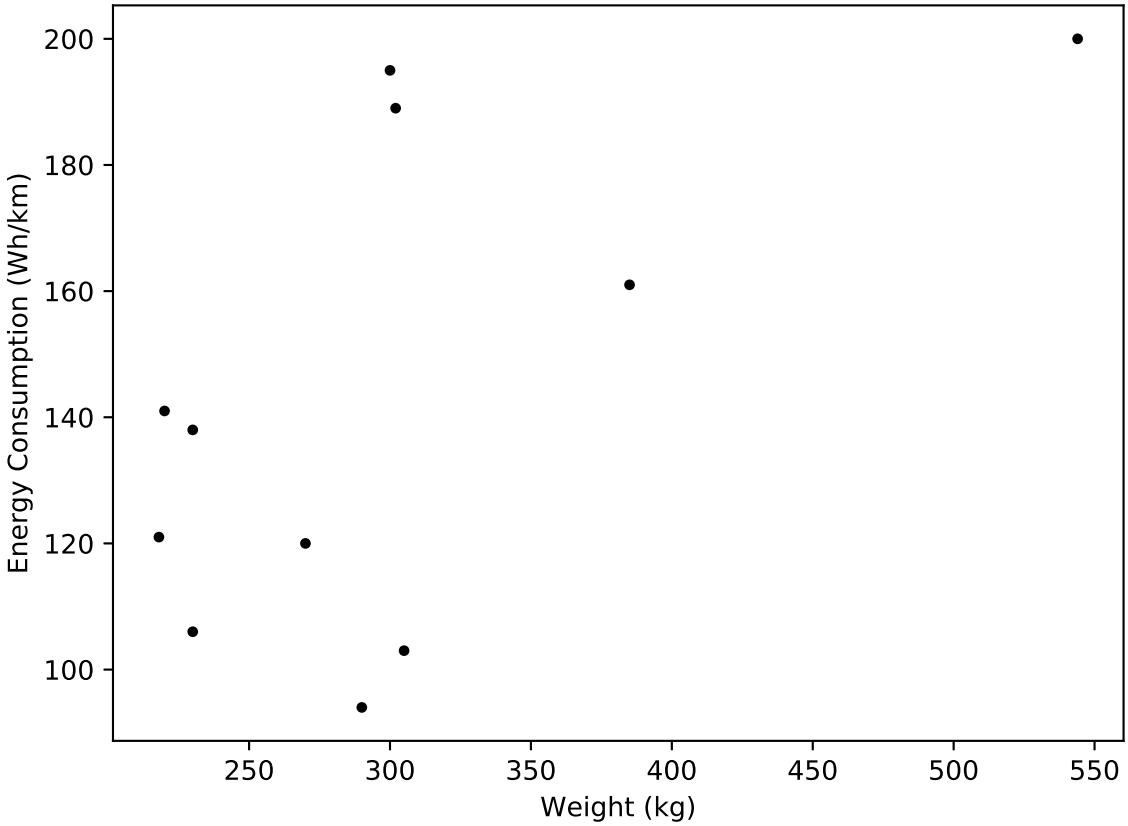

Fig. 1.1: Electric vehicle energy consumption per kilometer traveled vs. battery weight [15]

costly [14]. Dynamic charging can be used to increase the range of EVs without stopping to charge, thus allowing reduced battery size, or at least no further increase in battery size [6].

There are numerous studies which cover the electrical engineering aspect of inductive charging, both in static and dynamic applications [2,3,6,7]. In inductively coupled charging, DC power is converted to high frequency AC power and sent through the induction coils, which creates an oscillating magnetic field. A properly tuned receiver coil in close proximity to the transmitter coil will have AC current induced in it, which in a dynamic application can be used directly in the power train of an EV, or converted to DC for charging the battery [3].

1.2.1 Concrete Thermal Conductivity Studies

The current studies on the thermal conductivity of concrete are extensive, but due to

the numerous variations in cement types, mixture ratios, and aggregate types, it is still unlikely that a value found in literature will match the actual value of the concrete being used in experiments. For example, the values found in Sengul [16] are considerably lower than those found in Gandage [17], even though they both involve perlite. In addition to constituents affecting the thermal conductivity, the moisture level within the concrete also affects it, which has been studied in Tinker, Taoukil, Belkharchouche, and Gomes [13,18–20]. The different results that have been found are compiled in Table 1.1.

Table 1.1: Concrete thermal conductivity

Study	**Thermal Conductivity** W/(m K)	**Mixture/Type**
Taoukil [18]	0.2-1.2	Concrete with wood shavings
Belkharchouche [19]	0.1-2.6	Concrete with olive pomace
Jelle [21]	0.1-2.5	Structural Concrete
Zhang [22]	1.1-2.0	Varying levels of coarse and fine aggregate
Sengul [16]	0.1-0.7	Varying density of concrete using perlite and natural sand
Gandage [17]	0.7-3.1	Varying temperature and mixtures of fly ash and perlite
Jansson [23]	0.6-1.5	Varying temperature
Pia [24]	0.46	Fractal method for porous structures
Tasdemir [25]	0.1-0.6	Lightweight concretes of varying density
Kodur [26]	0.7-3.3	Varying temperature of NSC, HSC, SCC, and FAC
Toman [27]	1.1-2.8	Varying temperature of Temelin and Penly concrete

In all studies which included an analysis of moisture content, higher moisture content always resulted in increased thermal conductivity. Most studies presented here are focused on decreasing thermal conductivity for the purpose of increasing building efficiency [16, 17, 19–21]. Ideally, the experiments conducted in this application would use high thermal conductivity concrete. However, since there are other constraints on concrete

used for roadway construction [28], that may not be possible. Also, although aggregates are standardized [29], the cost of transporting aggregate could be significant due to its weight; thus most are obtained locally, if possible, resulting in slight variations of actual materials which could affect all properties of the resulting concrete. Thus, although there are many studies which could help understand the thermal conductivity of concrete, the actual thermal conductivity cannot be known without measuring it.

The studies mentioned in Table 1.1 show a wide range of thermal conductivity possible for concrete. In Taoukil, Belkharchouche, Jelle, and Gandage [17–19, 21], standard concrete had higher thermal conductivity than the specific type being studied. In Kodur [26], HSC had the highest thermal conductivity at low temperatures. One patent [30] estimates that the addition of silicon carbide as an aggregate to concrete can increase thermal conductivity; however, extensive study has not been conducted and silicon carbide is expensive to be used in this application. In all cases cited here aside from silicon carbide aggregate, the addition of other materials in place of or in addition to normal aggregate weakens concrete, and in most cases, also reduces thermal conductivity. Thus, none of the lower-conductivity concretes would be suitable for this application due to their lower strength alone. It is also not acceptable to use a slag cement or fly ash in concrete for this project, since both can contain metallic components such as iron or aluminum and thus interfere with the magnetic field generated by the induction coils [31]. A disadvantage to this restriction is that slag generally makes concrete more resistant to corrosion and weather [32–35].

1.2.2 Thermal Management Design

Although many systems are designed to run reliably at steady-state, systems that only periodically have a high thermal load can rely on the time it takes to heat up to prevent overheating [36]. A steady-state condition in this system would reach high temperatures due to the low thermal conductivity of concrete and the high heat generation within the system. Although it would be ideal to reach a low-temperature steady-state condition, such a design is not possible within the current constraints of the system. However, this system is also very unlikely to reach steady-state temperature conditions due to the periodic nature of

loading and the slow thermal response time. In dynamic charging, a single wireless charger would only be activated for a few seconds at a time [2–4, 6]. In static charging, depending on the power level attained, the charger would only be activated for around an hour at a time [1, 37, 38]. Thus, although an ideal steady-state cannot be reached, an adequate solution can be found.

With intermittent loading as described above, it is important to analyze the transient behavior of the system rather than just the steady-state behavior. In a transient system, heat capacity has great effect on the performance, as it affects how quickly the temperature of the system will increase. Due to the heat capacity of concrete [26], it can be a good place to store heat. However, due to the low thermal conductivity, its effectiveness as a thermal storage device is limited since the heat will not disperse within the material quickly enough to lower the temperature around critical components. In addition, due to low thermal conductivity, the possibility of cracking from thermal expansion is high when attempting to store heat. To prevent too high of thermal gradients within the concrete, and the possible resultant cracking of such thermal gradients, a phase change material (PCM) can be used to absorb heat at a constant temperature using latent heat of fusion.

There are multiple ways to implement a PCM into this system. One approach is to soak aggregate in melted PCM at a low pressure to fill voids in the aggregate with PCM rather than air [39, 40], then use that aggregate in the concrete. Another approach is to add microcapsules filled with PCM to the aggregate [41, 42]. Both of these methods are effective at increasing the heat capacity of the concrete. However, both also weaken the concrete [41] and do not improve the thermal conductivity [39, 42]. Soaking the aggregate in PCM reduces the thermal conductivity because of the low thermal conductivity of the PCM [39], and microcapsules have a similarly lower thermal conductivity due to the low conductivity of the PCM as well as an increase in air entrapment [42]. In order to take advantage of a PCM without weakening the concrete, reservoirs can be used [36]. In many cases, heat is channeled into the reservoir, which is sealed to prevent leakage due to the high thermal expansion of PCMs upon melting [36]. In this case, an exceptionally strong

container is unneeded, since it will be embedded in concrete.

CHAPTER 2

THERMAL CONDUCTIVITY MEASUREMENT

Accurate thermal modeling requires sufficiently accurate thermal properties. This chapter presents the method used in this thesis for determining thermal properties.

2.1 Common Methods of Thermal Conductivity Measurement

One very common method of determining thermal conductivity is to determine the heat capacity of a material using differential scanning calorometry (DSC), the density using thermo-mechanical analysis (TMA), and the thermal diffusivity using laser flash analysis (LFA). The thermal conductivity can then be determined by

$$k = \alpha \rho c_p \tag{2.1}$$

where k is the thermal conductivity, α is the thermal diffusivity, ρ is the density, and c_p is the specific heat of the material.

Since α, ρ, and c_p can be measured over a temperature range, the thermal conductivity can also thus be determined over a temperature range. Ideally, an accurate thermal model would include thermal properties that vary according to temperature accurately. A drawback to this method, however, is that it requires very small sample sizes. Some composite materials like those used in roadways have components which are much larger than the largest allowable sample size used in a DSC, TMA, and LFA setup. For example, this project requires the use and modeling of concrete, which is a composite material. For concrete with large aggregate, the large aggregate is much larger than the maximum sample size used in a DSC. Although the properties of individual components could be determined, the properties of all components combined cannot be simply or accurately modeled. Thus, this method cannot be used for concrete.

Other methods have been developed to determine conductivity of materials such as concrete [10]. One method is to place a sample between a hot and cold chamber. The method requires the sample to reach steady-state, and then the thermal conductivity can be determined by the equation

$$q'' = k\frac{T_1 - T_2}{L} \tag{2.2}$$

where q'' is the heat flux through the solid, T_1 is the temperature on the hot side, T_2 is the temperature on the cold side, and L is the sample thickness. This method requires good insulation on the sides since it is attempting to emulate 1-dimensional heat transfer. This method requires knowing the heat flux through the sample, however, which is difficult to know with the given setup. The stepped-bar apparatus is one version of this method, which uses multiple measurements of the temperature within the hot and cold chambers (which are made of aluminum) to more accurately determine the heat flux through the sample. A very large stepped-bar would have to be used for experiments on concrete, however, so this method was not chosen. Other methods are transient and require detailed knowledge of the heat capacity of the sample. As previously mentioned, the thermal properties of concrete vary greatly based on the mixture and moisture content, so reliance on a property that is not well known for the sample being tested is unacceptable.

2.2 Experimental Setup

The method used in this study is similar to the method with hot and cold chambers in that it attempts to simulate 1-dimensional conditions. However, the approach is to use a cylindrical sample rather than a flat plate. For testing of the method, it was first used on sand, then on concrete. The setup used a 7-inch long cylindrical heater with 1/4-inch diameter placed in the center of a 7-inch long section of cardboard concrete forming tube with a diameter of about 8 inches and about 2 mm thick. The volume in between was filled with the test material. A diagram of the setup is shown in Fig. 2.1

The diameter of the concrete forming tube was chosen in order to create a 3-inch thick continuous section of concrete. This is based on the requirement by ASTM standards that

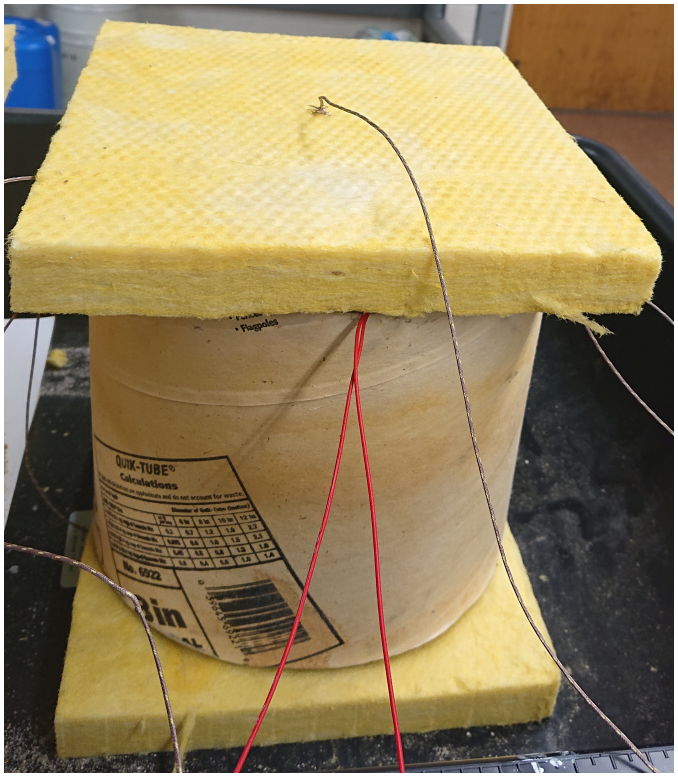

Fig. 2.1: Test setup for determining thermal conductivity of concrete

cylinders for testing compressive strength must be at least 3 times the diameter of the largest aggregate in the concrete [43]. Since the test standard from ASTM is designed to make the sample reflect the bulk properties of the concrete, it is assumed that adhering to similar standards will reflect bulk thermal properties of the concrete.For the concrete testing, the heater was covered with thermal paste to ensure minimal contact resistance between the heater and the concrete. A large reason for this was to ensure that the thermocouple which was measuring the surface temperature of the heater was accurate. The thermal conductivity of the cardboard tubing was measured using a stepped-bar apparatus, which is another form of emulating 1-dimensional conditions for thermal conductivity measurement.

With perfect insulation, this method would allow for the use of 1-dimensional analysis to estimate the thermal conductivity of the test material between the heater and the cardboard tube. Since the heat generation within the test is known, and with perfect insulation, no heat would be lost out the top or bottom of the test cylinder, the thermal conductivity

could be determined by measuring the temperature on the inside and outside of the test section, then using the cylindrical version of equation 2.2, which is

$$q'' = \frac{2\pi k(T_1 - T_2)}{\ln(r_2/r_1)} \tag{2.3}$$

with all variables defined as in equation 2.2, and r_1 as the radius of the hot cylinder surface and r_2 as the radius of the cold cylinder surface.

This 1-dimensional approach was used initially to design the test. However, the insulation used is not perfect, and in order to hold the weight of the concrete, it has a higher density than most insulating materials; and thus conducts heat better than many insulation materials. The use of this insulation makes the 1-dimensional analysis much less accurate, as a large percentage of heat escapes through the top and bottom. For this reason, a model of the experiment was developed in ANSYS Fluent using transitional flow (Transition SST) and energy models to most accurately model natural convection from the test body. Initially, these were the only models used. A radiation (Surface to Surface) model was also used to further increase accuracy.

The ANSYS model was set up to closely match the experimental setup. A picture of the model is shown in Fig. 2.2. An iterative process was used to adjust for immeasurable contact resistances which are present in the experiment. This iterative process also included adjustments to the thermal conductivity. This was accomplished by adjusting contact resistances and matching the temperatures at key points in the ANSYS model to those measured at those same key points on the experiment. The thermal conductivity is optimized to whatever value is required to match the temperatures measured at those key points. Boundary conditions were set using the recorded temperatures. Ambient air temperature was used as the boundary temperature for pressure inlets in the model, and the temperature at the bottom of the steel table was recorded and used as a constant temperature on the entire bottom surface of the table. Although this constant temperature assumption is not exactly true in all cases, the temperature was measured at multiple points below the experiment and found to be very close to the same temperature at every point measured.

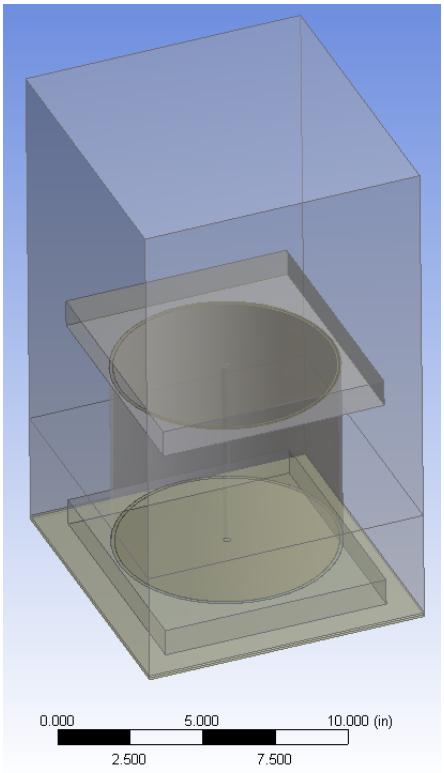

Fig. 2.2: Computer model of experimental setup

Although the accuracy of this method is highly dependent on the accuracy of the simulation models, it performs much better than the 1-dimensional analysis. This is because it requires fewer assumptions.

2.3 Results

The points used to compare results in the simulation and the test were as follows: The midpoint of the outer surface of the heater, the midpoint at the outer surface of the concrete, the midpoint at the outer surface of the cardboard, the center of the top of the upper and lower insulation blocks, below the center of the test section between the plastic tub and the steel table, and the lower surface of the steel table below the center of the test section. These points are highlighted in Fig. 2.3. There were also measurements taken on the upper insulation above the outer edge of the test section as well as the midpoint. This was done to ensure that the simulation was accurately representing heat loss throughout

the entire sample and not just at the middle. The same measurements were taken below the lower insulation section.

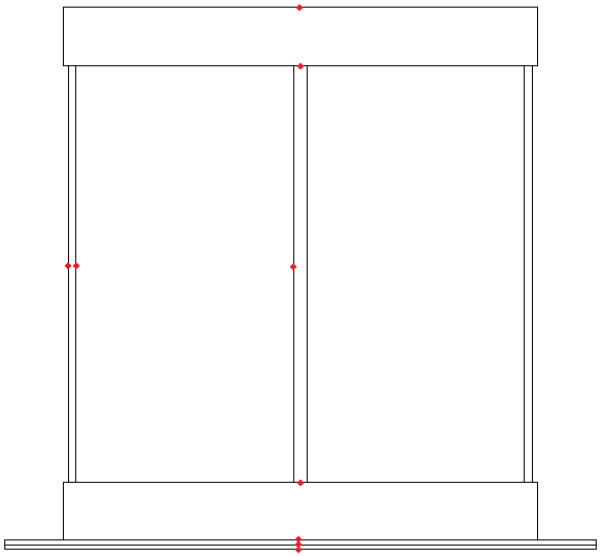

Fig. 2.3: Temperature probe placement

The most significant contact resistances were between the concrete and the cardboard, between the concrete and the insulation on the top, and the same interface on the bottom. Adjustments to the top and bottom contact resistances would shift the temperature readings found at the horizontal mid-plane by a constant, and adjustments to the thermal conductivity of the concrete would raise the outer temperatures along the mid-plane while leaving the center temperature very close to the same value because the heat flux through the concrete at steady state is very close to the same, independent of the thermal conductivity. Due to this, it was possible to adjust the contact resistances at the top and bottom until the temperatures along the vertical mid-plane matched, most importantly the temperature at the heater surface. At this point, the thermal conductivity could be adjusted until the concrete-cardboard interface temperature matched, and the contact resistance at that interface was adjusted to make the outer temperature match as well. After all of these steps, minor adjustments were then made to all values until all temperatures matched in

the simulation and experiment.

Initially, the temperatures measured in the experiment were significantly lower (2-4° C) than the simulation results. Increasing the contact resistances at the top and bottom or increasing the thermal conductivity of the insulation would decrease the temperature of the cylinder, but increase the temperature of the insulation, so adjustments could not bring the simulation temperatures into agreement with the experiment. For this reason, radiation was enabled in Fluent using the Surface-to-Surface model. I used a value of 0.8 for the emissivity of the insulation as well as the cardboard, which was based off of the emissivity of wood found on OptoTherm's website [44]. I used the same emissivity value because they are similarly colored.

The sample was allowed to reach a steady-state condition before using temperature measurements. However, to ensure that steady-state was reached, I logged the temperature of the key points from the time the heater was turned on until well after it reached steady-state conditions. The temperatures of the key points mentioned previously are shown in Fig. 2.4.

The heater input was measured to be 80 V and 0.2 A, giving a total power input of 16 W. To simulate the heater, this power was divided by the volume of the heater to get a volumetric heat generation value which was then assigned to the heater's geometry, which was set to have the same material properties as steel, since the outer shell of the heater is made from steel. The properties for each material used in the simulation are given in Table 2.1.

2.3.1 Cardboard Characterization

The thermal conductivity of the cardboard tubing was determined to be 0.21 $\mathrm{W/(m\,K)}$ using a stepped-bar apparatus. This value was assumed to be constant over the temperature range encountered in the testing. Although the thermal conductivity of many porous materials is a function of not only temperature, but moisture content, it was assumed that the moisture content of the cardboard and concrete would be identical due to them being bonded and in the same environment for an extended period of time. The density was

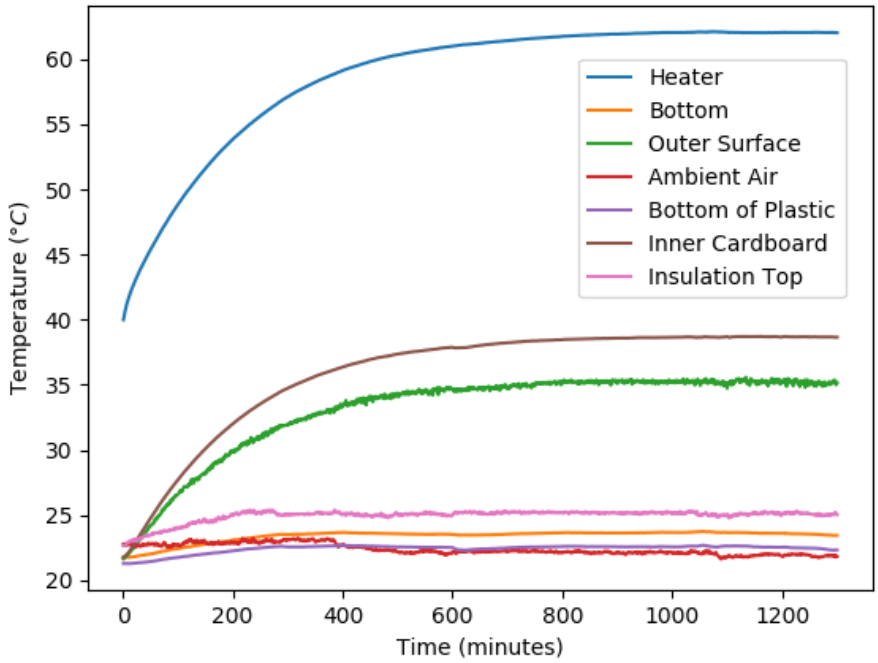

Fig. 2.4: Sample graph of temperature vs. time for heating of concrete sample

Table 2.1: Simulation material properties

Material	**Thermal Conductivity** $\mathrm{W/(m\,K)}$	**Density** $\mathrm{kg/m^3}$	**Specific Heat** $\mathrm{J\,kg^{-1}\,K^{-1}}$
Cardboard	0.21**	667*	1920*
Concrete	1.8*	2738*	775*
Insulation	0.131**	95.9*	700 [45]
Polyethylene	0.33 [46]	920 [46]	1900 [46]
Steel	16.27	8030	502.48

* indicates value was measured as part of this study
** indicates value was measured using stepped-bar apparatus
Citation indicates the source for properties not measured in this study

measured by cutting a sample and measuring its dimensions with a caliper, then measuring its mass. The density is then determined by

$$\rho = \frac{m}{V} \tag{2.4}$$

The heat capacity of this cardboard was determined by DSC. Although the heat capacity was determined for a temperature range from 0-100° C, the average value across the entire temperature range was used in this study. The heat capacity over the temperature range is shown in Fig. 2.5. A rise in heat capacity is noticeable in the room temperature region as well as nearing 100° C. As this is not a crucial element to this study, I will only speculate that these are due to a debonding agent (likely wax) on the inner surface of the concrete forming tube and the boiling point of the moisture within the cardboard, respectively.

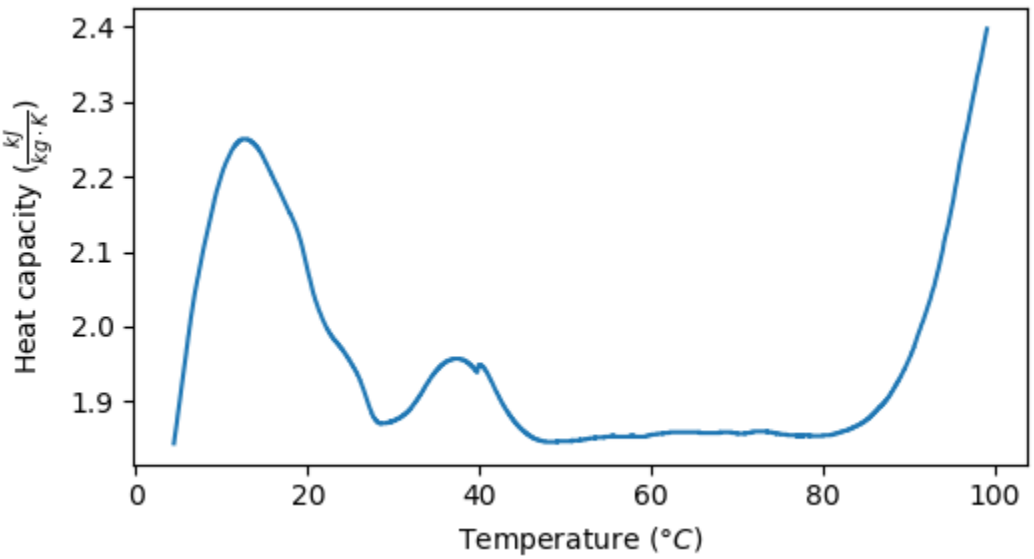

Fig. 2.5: Heat capacity of cardboard concrete forming tube vs. temperature

2.3.2 Insulation Characterization

The R-value given on the distributor's website for the insulation used in this experiment was 34 mW/(m K). This figure is flawed, however, because the distributor reports the exact same thermal resistance for insulation with only half of the density [47]. Most forms of thermal insulation work primarily by virtue of the low thermal conductivity of stagnant air [48], and the insulation works only because it prevents air flow and thus convection of the air within the insulation is restricted. Because the insulation material itself has a

much higher thermal conductivity, it is unlikely that a higher density board of the same material would not have a higher thermal conductivity due to reduced air content. Because of the unlikeliness of the reported thermal conductivity value being accurate, the thermal conductivity of the insulation was measured to be 0.131 $\mathrm{W/(m\,K)}$ using a stepped-bar apparatus.

2.3.3 Concrete Characterization

The thermal conductivity of the concrete was determined to be 1.8 $\mathrm{W/(m\,K)}$ through this experiment. The density was calculated by measuring the dimensions and the weight and using equation 2.4. The heat capacity was calculated by performing a transient simulation and comparing the response time to the measured response time, then adjusting the heat capacity of the concrete until the heating curves matched. This matching heating curve is shown in Fig. 2.6. Examining the figure, both the experimental and simulated are very similar to each other in the first portion, which is most critical. There is, however, a small sudden decrease in temperature of the experiment. This is due to ambient temperature drop. If this temperature drop were accounted for, the curve would match more closely that of the simulation. Although this could be more finely tuned, it is sufficient to know that the heat capacity of this concrete is close to 775 $\mathrm{J/(kg\,K)}$

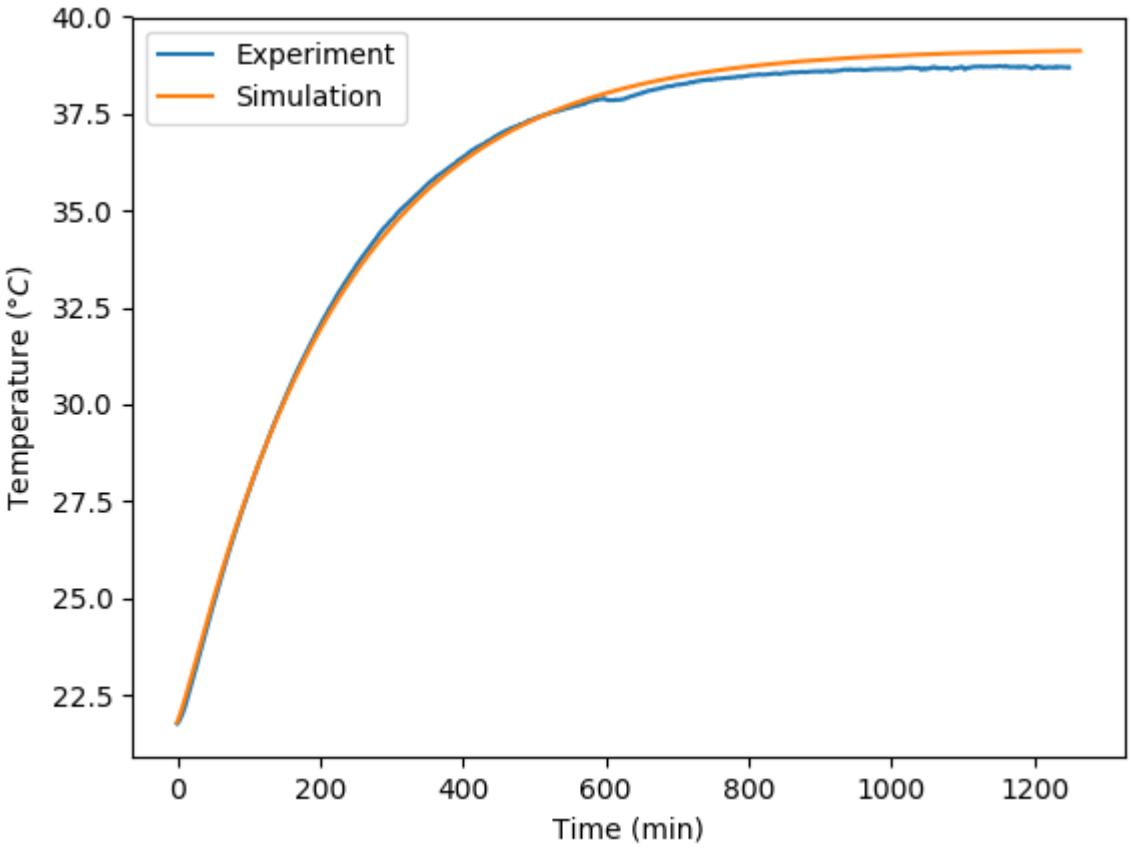

Fig. 2.6: Comparison of concrete sample heating over time for simulation and experiment

CHAPTER 3

CONCRETE EMBEDDED THERMAL MODEL

This chapter describes the creation and use of ANSYS models to accurately characterize the thermal behavior of concrete embedded induction coils as well as experimental validation of the model.

3.1 Coil Construction

Because a simulation model is used to predict the thermal behavior of the system in many different conditions which would be impractical to test for, it is important to know that the computer model is accurate in conditions which can be tested for. To ensure this, a concrete slab with embedded coils was constructed, and a computer model which closely resembles the physical setup was also made. Most of the design choices for this pad are the subject of other studies which have to do with stress and electromagnetic considerations and only minimally affected by the thermal design of the pad. Since this study is only concerned with the thermal aspect of the design, it is sufficient to simply mention the design and the corresponding computer model. The design is shown in Fig. 3.1.

Rather than embedding temperature sensors in the concrete, PVC tubes were placed in the concrete to leave holes in the concrete so that key points could be accessible for temperature sensors later.

Because this study is also concerning ways to improve thermal management of roadway embedded systems, a comparison is also made between a slab with a phase change material encasing the ferrite components of the charging assembly and one without. A computer model of both is also used for comparison and validation of both cases.

Fig. 3.1: Induction coils before concrete was poured

3.2 Simulation Model

A model was made in ANSYS to closely resemble the actual constructed slab. A picture of the model is shown in Fig. 3.2. There are small differences between the computer model and the physical model. The most important difference is that in the computer model, the coils themselves are four separate loops, whereas in the physical model, all four loops are made from a single cable. The computer model was made this way for simplicity and because it does not have a large effect on any important aspects of the study.

3.2.1 Material Properties

In addition to concrete, other materials are used in this simulation. Notably, the Litz wire is made mostly of copper, the insulation around it is rubber, ferrite is a critical component of the induction coils, paraffin wax is used to absorb heat, and the entire assembly is held together using polypropylene. The concrete is also reinforced with fiberglass. The

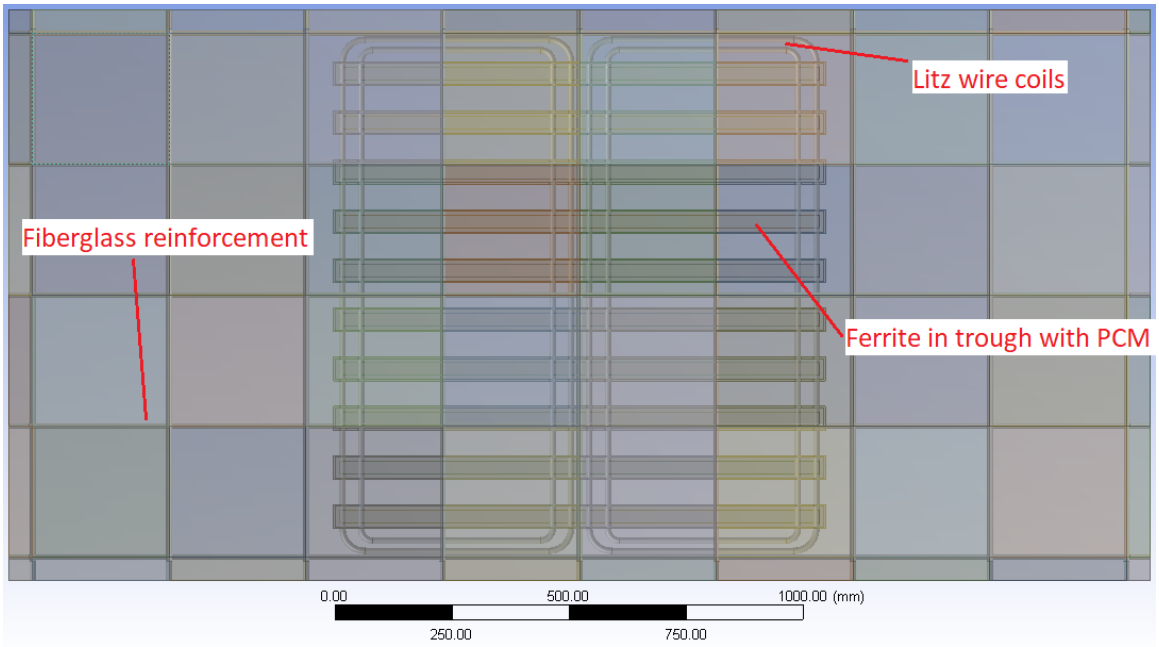

Fig. 3.2: Simulation model of coils embedded in concrete

relevant properties of these materials will be discussed hereafter. A summary of these properties is found in Table 3.1.

Table 3.1: Coil simulation material properties

Material	**Thermal Conductivity** $\mathrm{W/(m\,K)}$	**Density** $\mathrm{kg/m^3}$	**Specific Heat** $\mathrm{J\,kg^{-1}\,K^{-1}}$
Concrete	1.8	2738	775
Aggregate	1.55	2203	1407
Paraffin Wax	0.26 (solid)-0.16 (liquid)	800-900	2470-28880
Wire Insulation	0.37	1070	1540
Fiberglass Reinforcement	0.93	1850	565
Wire Copper	40 (radial)	4116	385
Ferrite	4	4600	750

Values for the thermal properties of aggregate were taken from Howlader [49] and averaged to find the values used here. The thermal conductivity is on average 1.55 $\mathrm{W/(m\,K)}$,

the density is 2203 kg/m^3, and the specific heat is 1407 J/(kg K). These values may be unrealistically high, however, as other sources show much lower values [50].

A value from Kenisarin [51] was used for the thermal conductivity of paraffin wax in both the liquid and solid phases. Since the melting temperature of these waxes varies based on the paraffin chain length, the exact melting temperature was measured using DSC. The purpose of using wax is to absorb heat. In order to accurately model this heat absorption, it is necessary to know the heat capacity of the wax over the range of temperatures that it will experience. Although there is a difference between the heat capacity and the latent heat of fusion when going through melting, the effect of absorbing heat is the same, therefore this difference is ignored. The heat capacity over a temperature range of 5-100° C is given in Fig. 3.3. Because testing occurred at lower than 5° C, the remaining heat capacity is extrapolated from the value at the lowest temperature. The density was determined by taking the density of a different paraffin wax [52] with a lower melting temperature and shifting the density values to match the melting point of the paraffin used in this study. See Fig. 3.4.

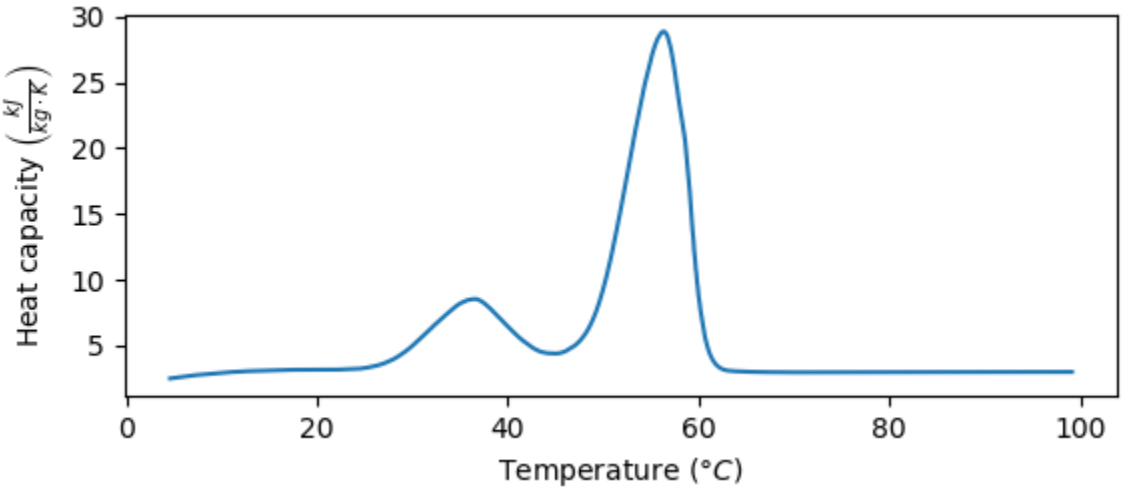

Fig. 3.3: Heat capacity of paraffin wax vs. temperature

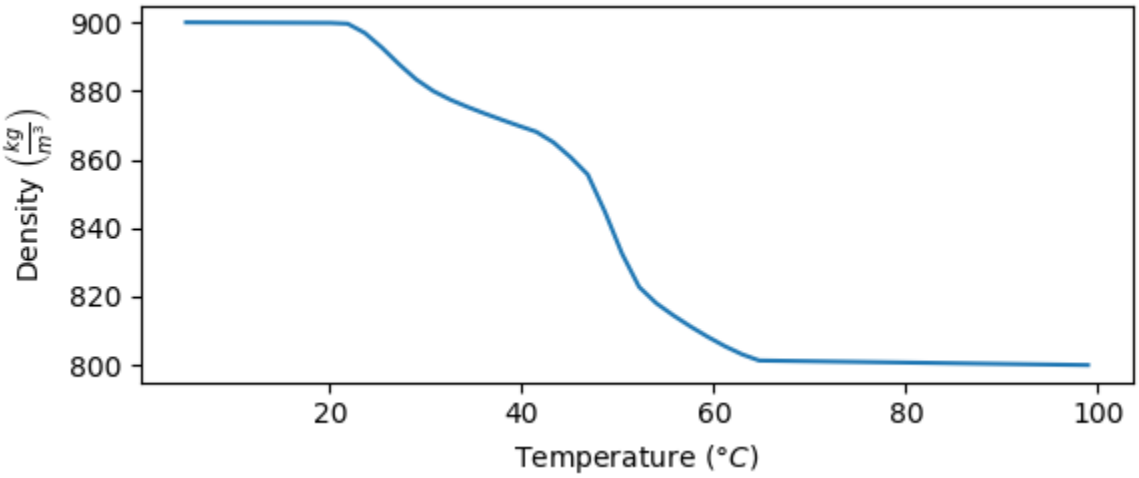

Fig. 3.4: Density of paraffin wax vs. temperature

The provider of the Litz wire only specified that this insulation was a thermoplastic elastomer and did not give any thermal properties of the material. Because of this, the thermal conductivity of the insulation around the Litz wire was measured to be 0.37 W/(m K) using a stepped-bar apparatus. The density of the insulation was measured as 1070 kg/m^3. The heat capacity of this material was determined using DSC to be 1540 J/(kg K) on average.

Thermal conductivity of fiberglass reinforcement was measured to be 0.93 W/(m K) using the stepped-bar apparatus. The density is measured as about 1850 kg/m^3, and the heat capacity is about 565 J/(kg K).

Because the electrical conductor is not pure copper, but rather a weave of very small copper wires, its density is much different from that of pure copper. The manufacturer reported a wire density of 4116 kg/m^3, which was verified by measurement to be accurate. The thermal conductivity in the radial direction of the wire is also not that of pure copper, due to the individual strands as well as the insulation on each strand. A lower estimate was used, but this number was still much higher than the other materials used in the simulation, so any heat generated in the Litz wire is conducted to the outer insulation much more quickly than it can be conducted out of the insulation. The heat capacity could

not be measured, so the value of copper was used, and I relied on the modified density to produce an accurate simulation.

Values for the thermal properties of ferrite were taken from standard ANSYS values. Thermal conductivity is 4 W/(m K), density is 4600 kg/m^3, and specific heat is 750 J/(kg K).

3.2.2 Boundary and Load Conditions

Boundary conditions were based on physical reality and designed to simulate that reality. The top and side surfaces of the slab was set to have a variable convection coefficient based on the temperature difference between the ambient temperature and the surface of the slab, based on horizontal and vertical flat plate convection correlations given by Incopera et al. [53]. A 2-ft. deep section of aggregate was placed under the slab, and the bottom of the aggregate set to a constant temperature of 0°C. This is to properly simulate the relatively unchanging nature of the in-earth temperature while still allowing the ground to heat up if necessary.

The convection coefficients for both vertical and horizontal plates were calculated using a Python script with material properties given by Incopera et al. [53], which is shown in Appendix A.1. The temperature dependent convection coefficients are shown in Fig. 3.5. Because the ambient temperature did not vary greatly during testing, it is reasonable to assume that the material properties of the air also did not vary greatly. These variations are mostly handled in the original calculation of the convection coefficient and the way the coefficient is used in ANSYS, since the material properties are calculated based on the film temperature, which changes based on the surface temperature.

The load was determined by using a simple simulation setup in ANSYS Maxwell. The coils were cut along a single plane to allow for assignment of electrical current. The actual current through the coils in testing was 115 A, thus the same current was applied to the simulation. Core losses were also calculated in the ferrite. The electromagnetic properties used for ferrite are given in Table 3.2. C_m, X, and Y are temperature dependent parameters, but for this initial work, they were calculated for standard room temperature and remained the same for all stages of simulation.

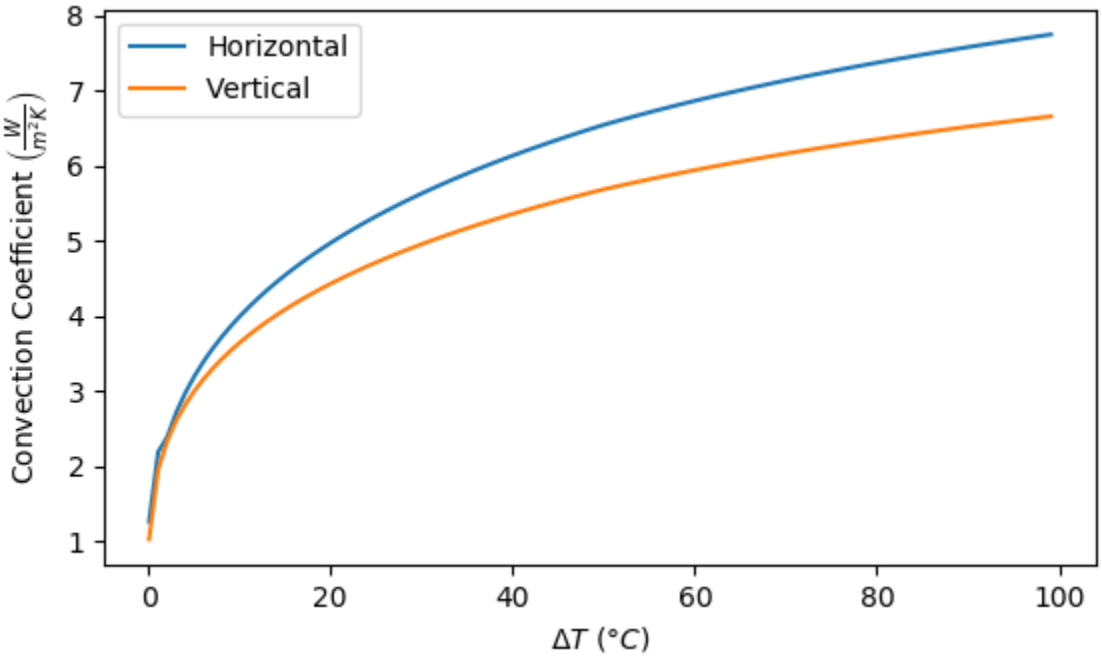

Fig. 3.5: Convection coefficients for horizontal and vertical flat plates vs. temperature difference between surface and ambient air

Table 3.2: Ferrite and copper electromagnetic properties

Property	**Ferrite**	**Copper**
Relative Permittivity	12	1
Relative Permeability	3000	0.999991
Bulk Conductivity	0.01 $\mathrm{S\,m^{-1}}$	10600000 $\mathrm{S\,m^{-1}}$
C_m	12.9409727037054	No core loss
X	1.2843639309547	No core loss
Y	2.45714981526881	No core loss
Density	4800kg/$\mathrm{m^3}$	8933 kg/$\mathrm{m^3}$

The resulting heat loads from the electromagnetic simulation were imported to a transient thermal simulation in ANSYS Mechanical, where all material properties listed in the previous subsection were used. This allows for a comparison between the simulation model and the actual model, which will enable better thermal design and analysis.

3.3 Results

Because wireless power transfer systems generate strong magnetic fields, it was not possible to use thermocouples to measure temperature like were used in chapter 2 of this thesis. Instead, fiberoptic temperature sensors were used because they would not be affected by the magnetic fields. Unlike the thermocouples, however, these probes had a 6-inch long ceramic sleeve around them for protection.

Temperature probes were placed in the locations indicated in Fig. 3.6. These are the exact locations whose temperature is reported from the simulation, and the temperature probes were placed in the experiment as close as possible to these locations. Due to the method of placing the probes, they are not exactly in these places. In the simulation setup, the coils are all separate bodies, but in the experiment it is all a single wire wound into a double-D shape. Because of this, the temperature probe in the experiment is actually on the coil where it crosses from one loop to another in the center of the pad.

Because the temperature probes are 6-inches long and the point they are measuring is only approximately 2 inches from the top surface, at least half of each probe is outside the concrete. In order to mitigate the effect this has on the temperature reading, insulation was placed on the probe in the portions not in the concrete. A tarp was used to cover the entire slab during testing to reduce convection due to wind. It also reduces direct influence of radiation from the sun.

The simulation initially produced results considerably lower than the measured temperature, which is the opposite of what I expected, since the temperature probes read lower than the actual temperature in this setting due to half of the probe being outside of the concrete. The temperature shown in Fig. 3.7 is a comparison of the temperature over time at the points measured in both the simulation and in the experiment. Matching colors indicate matching temperature reading locations, and the thin and thick lines are the simulation and experimental data, respectively.

As can be seen in Fig. 3.7, most of the temperature curves are considerably different from their experimental counterparts. Overall, it appears that the likely causes for all dis-

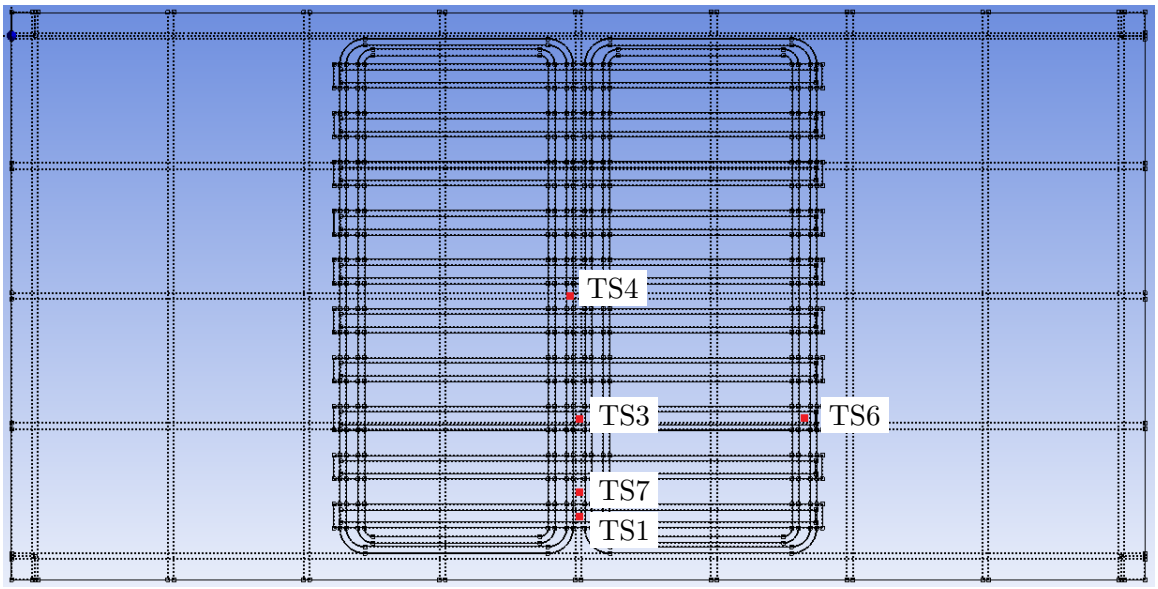

Fig. 3.6: Temperature sensor locations for both simulation and experiment with PCM

crepancies are that the heat is being removed from the simulation too quickly, either by convection or conduction, that the heat is not being generated at the rate the electromagnetic simulation estimates it to be, there are significant contact resistances not accounted for in the simulation, or the heat capacity of the concrete is incorrect.

Although TS1 reaches a similar temperature at the time the power was turned off, the simulation heats up considerably faster than the experiment. TS3 shows similar behavior, except that the temperatures match at a much sooner time. All other sensors appear to either not be heating up fast enough in the simulation due to either excessively high heat capacity or high heat extraction from the boundary conditions.

Because of the difference in the simulation and the experiment, it appears that some part of the simulation must be incorrect. Different causes will be explored hereafter, beginning with heat capacity. A simulation with a heat capacity of 500 $\mathrm{J/(kg\,K)}$ in the concrete appears to increase the maximum temperature the simulation would reach if it were to run until steady-state; however, it also initially heats up much more quickly than the experiment did. This is shown in Fig. 3.8. Therefore, it is likely that a difference of heat capacity is contributing to the difference in simulation and experimental results. Furthermore, because

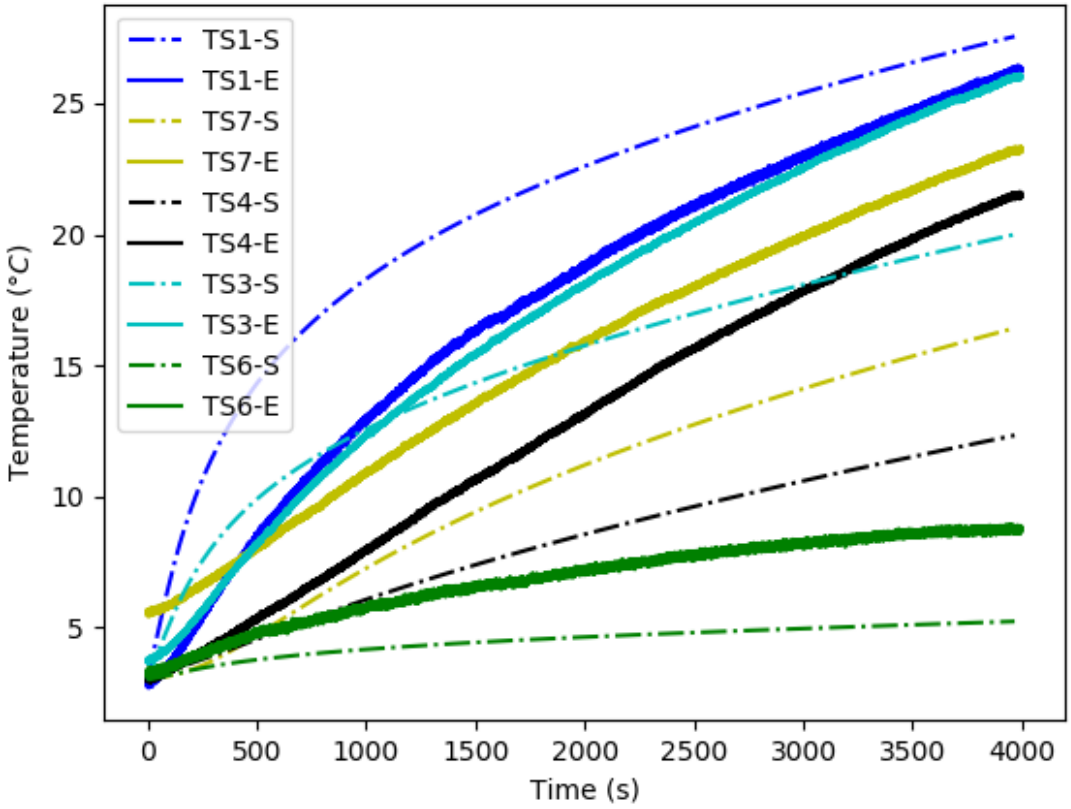

Fig. 3.7: Comparison of simulation and experimental measured temperatures for slab with PCM

the concrete studied in Chapter 2 of this thesis was stored in a different environment than the concrete in these experiments, the moisture levels within the concrete could be much different, despite them being from the same batch. The moisture level directly affects the heat capacity of concrete, as mentioned before [13].

Similarly, the thermal conductivity of the concrete may be different from what was determined in Chapter 2 because of different moisture levels. A simulation with a lower conductivity of 1.2 W/(m K) in the concrete shows similar behavior to the simulation with lower heat capacity, as shown in Fig. 3.9. Since concrete makes up the bulk of the slab, this is as expected since the thermal response is described by the Fourier number, which is defined as

$$Fo = \frac{kt}{c_p \rho L^2} \tag{3.1}$$

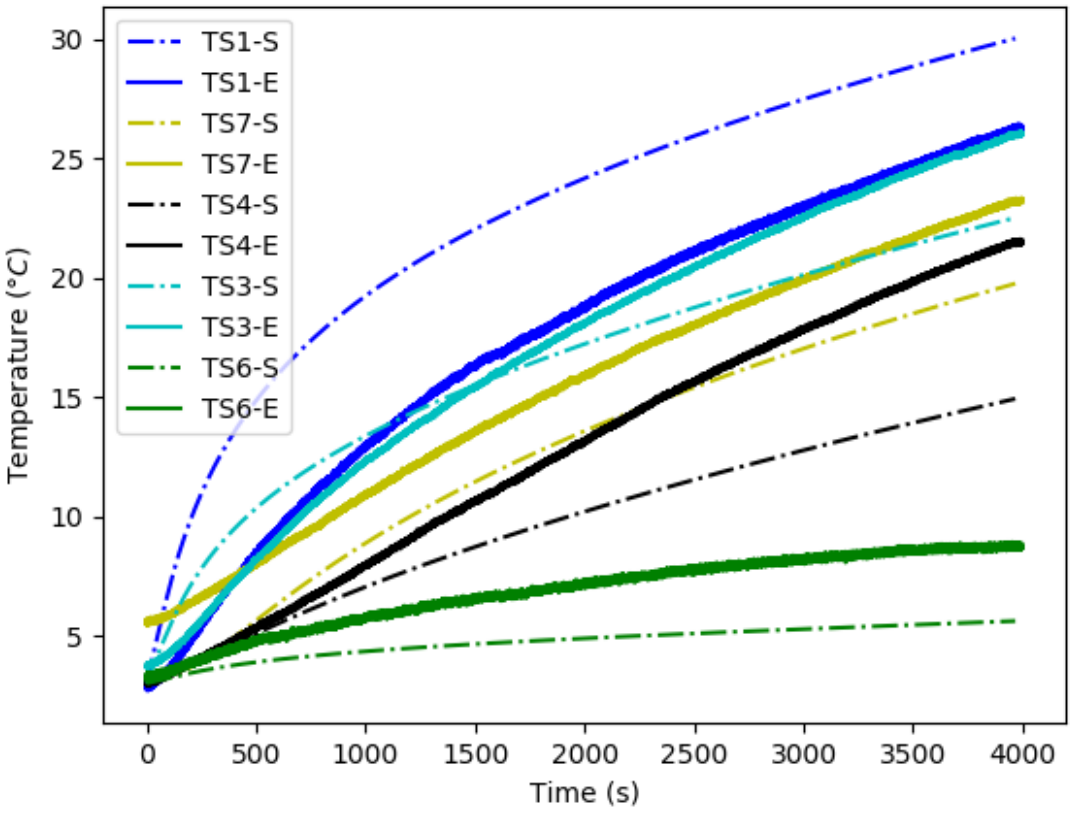

Fig. 3.8: Comparison of simulation and experimental measured temperatures for slab with PCM and lower heat capacity

which shows that increasing the heat capacity has the exact same effect on the thermal response as decreasing the thermal conductivity.

It is possible that there are significant contact resistances which are unaccounted for in the simulation. It is assumed that everything bonded well to the concrete, thus there is no contact resistance accounted for. This may be a flaw in the simulation design, as it is not known how well all components bonded to each other.

Another possible cause of low steady-state temperatures is excessive heat extraction from the simulation environment. To explore the possible effect of the boundary conditions, a simulation with an insulating boundary rather than convection on top of the slab was used. The results ended up being almost identical to results obtained by convection, which shows that in the time the experiment ran for, the simulation did not release much heat through

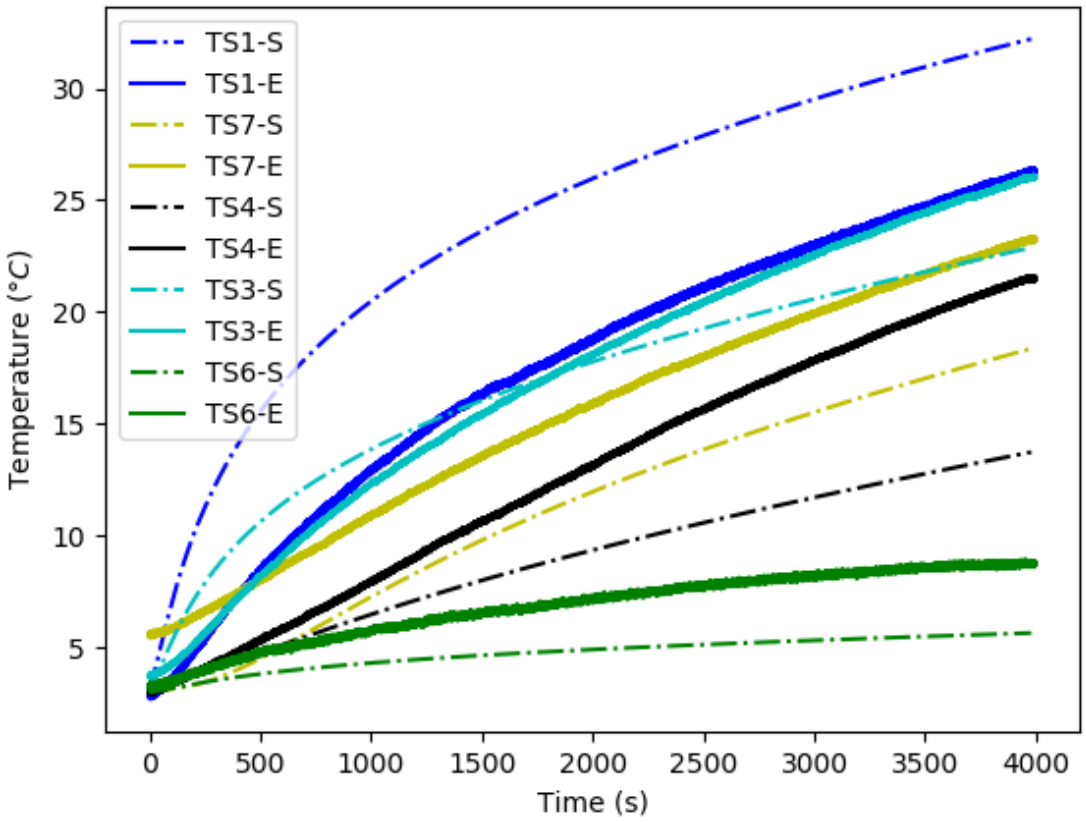

Fig. 3.9: Comparison of simulation and experimental measured temperatures for slab with PCM and lower thermal conductivity

the top. The sides are too far away to have a significant impact thermally within that same time frame.

There is no radiation accounted for in this simulation, although the experiments were conducted outside. This means that the top surface has less heat entering it than in reality, which could affect the temperature readings since the temperature sensors are in the top two inches of the slab. There is also a possibility that radiation from the sun heats up the temperature sensors themselves thus causing them to read higher temperatures than they should.

The slab without PCM is shown in comparison with the pad with PCM in it in Fig. 3.10 as a demonstration of the improvement of the thermal response time by adding PCM. The temperatures have been shifted to have similar starting temperatures for better comparison.

All temperatures are higher in the non-PCM slab than in the PCM slab except for two. All temperatures of the slab with PCM would level off to lower temperatures than the non-PCM slab would if the test were conducted for longer.

It is helpful to note that this comparison is done well below the melting temperature of the PCM. As is shown in Table 3.1, the heat capacity of the PCM is always higher than that of concrete by a large amount. If testing were to reach the melting temperature of the PCM (see Fig. 3.3), there would be a significant plateau in the PCM slab at least for the temperatures around the ferrite bars, where the PCM is located.

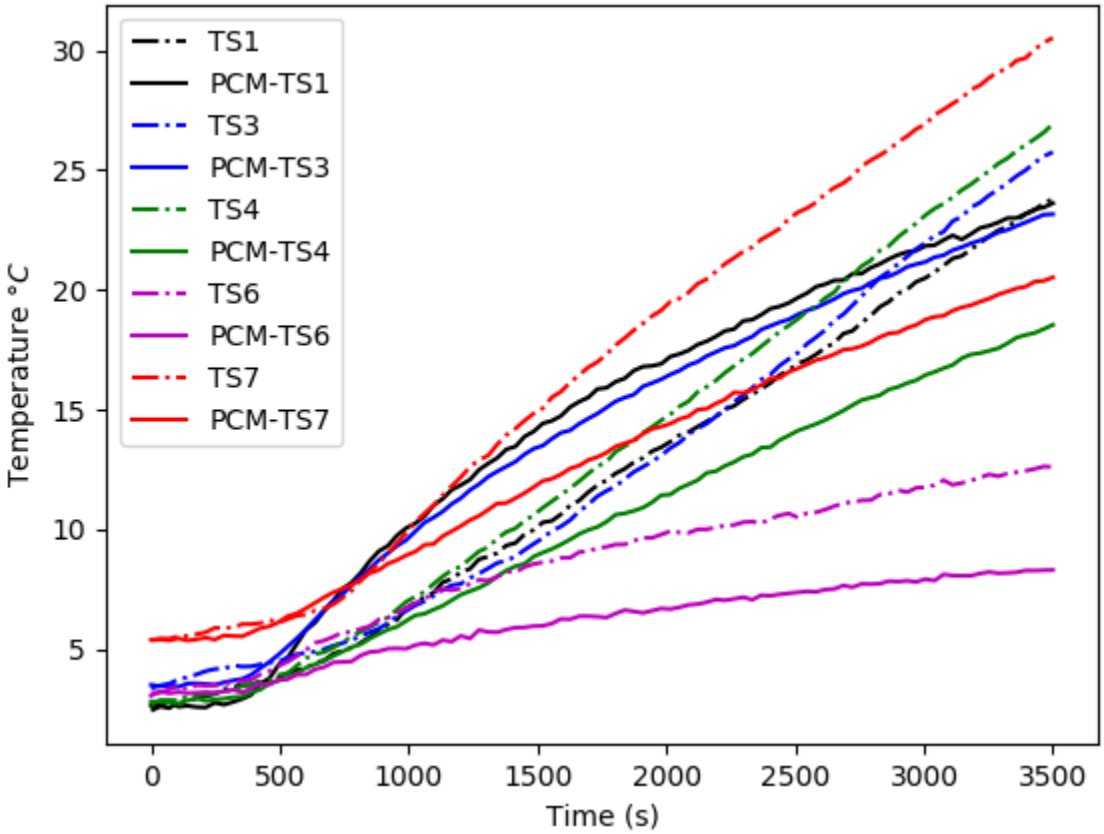

Fig. 3.10: Experimental temperature vs. time of both PCM and non-PCM slabs

CHAPTER 4
CONCLUSIONS

This study has underlined multiple reasons and requirements for embedding wireless charging systems in roadways.

4.1 Review of this Work

Wireless charging has potential to simplify the charging of electric vehicles as well as expand opportunities for charging. Embedding charging coils in roadways and parking stalls allows for seamless and easy charging in more situations than currently available. This charging potential can greatly decrease range anxiety for electric vehicle users.

An accurate study of the thermal aspects of embedded charging coils requires accurate knowledge of the thermal properties of the materials used in the system. This study has outlined a method of determining the average thermal conductivity and average heat capacity of materials that are of a necessity larger than methods such as DSC will allow. One of the major advantages of this method is its low cost. Provided adequate simulation software is available, it requires minimal equipment.

Simulating a full model presents its own challenges, the greatest of which is creating a model that accurately represents the real system. Creating ports to insert temperature sensors was a poor method of temperature measurement. The length of the probes combined with their inherent thermal conductivity causes uncertainty in the measurements because heat is extracted by convection through the probe's ceramic protective sheath. This effect would not be so severe if the entire sheath were in the concrete, but in this setting the sheath was halfway out of the concrete.

4.2 Potential Future Work

This study has only introduced ways to study the thermal management of concrete embedded induction coils. There are many ways to get improved results from future studies as well as ways this work can be expanded upon. Future work should use smaller temperature probes, eliminating uncertainty about what point the temperature is being read at, as well as preventing heat conduction along the probe. In addition, temperature probes should be embedded in the concrete along with the components whose temperature they are measuring, thus ensuring heat is not escaping by a route which would not exist without the temperature probe. In particular, it prevents the temperature sensor from reading a lower temperature than it should.

Future simulations should include temperature dependent heat generation within the electromagnetic simulation. Thermal simulations should include temperature dependent properties to the extent possible.

Future work should also include cyclic testing to better reflect how the charging pads would be used in practice. Testing should also be done for longer periods of time to better understand how embedded coils would perform as a docking station for static charging. It is also essential to test embedded coils under stress loading as well as thermal loading to better understand what the limits of a system embedded in concrete are.

Other possibilities that should be explored are whether it is viable to embed power electronics within the concrete as well as the coils, where they would need to be placed physically, and what method of thermal management that would require. Such studies must also take into account electrical and structural aspects of the entire system.

REFERENCES

[1] Forward, E., Glitman, K., and Roberts, D., "An Assessment of Level 1 and Level 2 Electric Vehicle Charging Efficiency," *Vermont Energy Investment Corportation*, 2013.

[2] Cirimele, V., Diana, M., Freschi, F., and Mitolo, M., "Inductive Power Transfer for Automotive Applications: State-of-the-Art and Future Trends," *IEEE Transactions on Industry Applications*, Vol. 54, No. 5, 2018.

[3] Bi, Z., Kan, T., Mi, C. C., Zhang, Y., Zhao, Z., and Keoleian, G. A., "A Review of Wireless Power Transfer for Electric Vehicles: Prospects to Enhance Sustainable Mobility," *Applied Energy*, Vol. 179, 2016.

[4] Hutchinson, L., Waterson, B., Anvari, B., and Naberezhnykh, D., "Potential of Wireless Power Transfer for Dynamic Charging of Electric Vehicles," *IET Intelligent Transport Systems*, Vol. 13, 2019.

[5] Suh, I. S., "Application of Shaped Magnetic Field in Resonance (SMFIR) Technology to Future Urban Transportation," *Interdisciplinary Design: Proceedings of the 21st CIRP Design Conference*, 2011.

[6] Throngnumchai, K., Hanamura, A., Naruse, Y., and Takeda, K., "Design and Evaluation of a Wireless Power Transfer System with Road Embedded Transmitter Coils for Dynamic Charging of Eletric Vehicles," *2013 World Electric Vehicle Symposium and Exhibition*, November 2013.

[7] Russer, J. A., Dionigi, M., Mongiardo, M., Costanzo, A., and Russer, P., "An Inductive Power Transfer Highway System for Electric Vehicles," *IEEE CALCON 2014*, November 2014.

[8] Kim, S., Amirpour, M., Covic, G., and Bickerton, S., "Thermal Characterisation of a Double-D Pad," *IEEE MTT-S Wireless Power Transfer Conference (WPTC)*, June 2019.

[9] Hwang, K., Chun, S., Yoon, U., Lee, M., and Ahn, S., "Thermal Analysis for Temperature Robust Wireless Power Transfer Systems," *IEEE Wireless Power Transfer*, May 2013.

[10] Asadi, I., Shafigh, P., Hassan, Z. F. B. A., and Mahyuddin, N. B., "Thermal Conductivity of Concrete – A Review," *Journal of Building Engineering*, Vol. 20, 2018.

[11] Lee, H.-S. and Kwon, S.-J., "Effects of Magnetite Aggregate and Steel Powder on Thermal Conductivity and Porosity in Concrete for Nuclear Power Plant," *Advances in Materials Science and Engineering*, Vol. 2016, No. 9526251, 2016.

[12] Tinker, J. A. and Cabrera, J. G., "Modeling the Thermal Conductivity of Concrete Based on its Measured Density and Porosity," *Buildings V Proceedings*, 1992, pp. 91–95.

[13] Tinker, J. A., Cabrera, J. G., and Ganjian, E., "Thermal Conductivity of Concrete: Effect of Moisture," *Building Serv. Eng. Res. Technol.*, Vol. 13, 1992.

[14] Adair, D., Ismailov, K., and Bakenov, Z., "Thermal Management of Lithium-ion Battery Packs," 2014.

[15] Berjoza, D. and Jurgena, I., "Influence of Batteries Weight on Electrical Automobile Performance," *Engineering for Rural Development*, Vol. 24, 2017.

[16] Sengul, O., Azizi, S., Karaosmanoglu, F., and Tasdemir, M. A., "Effect of expanded perlite on the mechanical properties and thermal conductivity of lightweight concrete," *Energy and Buildings*, Vol. 43, 2011.

[17] Gandage, A. S., Rao, V. R. V., Sivakumar, M. V. N., Vasan, A., Venu, M., and Yaswanth, A. B., "Effect of Perlite on Thermal Conductivity of Self Compacting Concrete," *Procedia - Social and Behavioral Sciences*, Vol. 104, 2013.

[18] Taoukil, D., bouardi, A. E., Sick, F., Mimet, A., Ezbakhe, H., and Ajzoul, T., "Mousture Content Influence on the Thermal Conductivity and Diffusivity of Wood-Concrete Composite," *Construction and Building Materials*, Vol. 48, 2013.

[19] Belkharchouche, D. and Chaker, A., "Effects of Moisture on Thermal Conductivity of the Lightened Construction Material," *International Journal of Hydrogen Energy*, Vol. 41, 2017.

[20] Gomes, M. G., Flores-Colen, I., Manga, L. M., Soares, A., and de Brito, J., "The influence of moisture content on the thermal conductivity of external thermal mortars," *Construction and Building Materials*, Vol. 135, 2017.

[21] Jelle, B. P., "Traditional, state-of-the-art and future thermal building insulation materials and solutions – Properties, requirements and possibilities," *Energy and Buildings*, Vol. 43, 2011.

[22] Zhang, W., Min, H., Gu, X., Xi, Y., and Xing, Y., "Mesoscale Model for Thermal Conductivity of Concrete," *Construction and Building Materials*, Vol. 98, November 2015.

[23] Jansson, R., "Measurement of Concrete Thermal Properties at High Temperature," *Proceedings from the fib Task Group 4.3 workshop "Fire Design of Concrete Structures: What now? What next?"*, December 2004.

[24] Pia, G. and Sanna, U., "A geometrical fractal model for the porosity and thermal conductivity of insulating concrete," *Construction and Building Materials*, Vol. 44, 2013.

[25] Tasdemir, C., Sengul, O., and Tasdemir, M. A., "A comparative study on the thermal conductivities and mechanical properties of lightweight concretes," *Energy and Buildings*, Vol. 151, 2017.

[26] Kodur, V. and Khaliq, W., "Effect of Temperature on Thermal Properties of Different Types of High-Strength Concrete," *Journal of Materials in Civil Engineering*, Vol. 23.

[27] Toman, J. and Cerny, R., "Thermal Conductivity of High Performance Concrete in Wide Temperature and Moisture Ranges," *Acta Polytechnica*, Vol. 41, No. 1, 2001.

[28] Utah Department of Public Transportation, *2017 Standard Specifications for Road and Bridge Construction*, January 2017.

[29] Kosmatka, S. H. and Panarese, W. C., *Design and Control of Concrete Mixtures*, Portland Cement Association, 2016.

[30] et al., B., "Cementitious Composite Material with Silicon Carbide Aggregate," September 1985.

[31] Zhang, K., Li, B., and Wu, W., "Structural and magnetic properties of steel slag based glass–ceramics," *Advances in Applied Ceramics*, Vol. 114, No. 2, 2015.

[32] "Mitigating Alkali-Silica Reaction," *Slag Cement in Concrete*, , No. 8, 2013.

[33] "Reducing Permeability," *Slag Cement in Concrete*, , No. 6, 2013.

[34] "Mitigating Sulfate Attack," *Slag Cement in Concrete*, , No. 7, 2013.

[35] "Reducing Thermal Stress in Mass Concrete," *Slag Cement in Concrete*, , No. 9, 2013.

[36] Fleischer, A. S., *Thermal Energy Storage Using Phase Change Materials Fundamentals and Applications*, Springer, 2015.

[37] Collin, R., Miao, Y., Yokochi, A., Enjeti, P., and von Jouanne, A., "Advanced Electric Vehicle Fast-Charging Technologies," *Energies*, Vol. 12, No. 1839, 2019.

[38] Chehab, N., "Pump up the Charge with Extreme Fast Charging," U.S. Department of Energy, https://www.energy.gov/eere/articles/pump-charge-extreme-fast-charging, 2017.

[39] Niall, D., Kinnane, O., West, R., and McCormack, S., "Mechanical and thermal evaluation of different types of PCM-concrete composite panels," *Civil Engineering Research in Ireland Conference*, 2016.

[40] Umar, H., Rizal, S., Riza, M., and Mahlia, T. M. I., "Mechanical properties of concrete containing beeswax/dammar gum as phase change material for thermal energy storage," *AIMS Energy*, Vol. 6, 2018.

[41] a Fenollera, M., Miguez, J. L., Goicoechea, I., Lorenzo, J., and Alvarez, M. A., "The Influence of Phase Change Materials on the Properties of Self-Compacting Concrete," *Materials*, 2013.

[42] Narain, J., Jin, W., Ghandehari, M., Wilke, E., Shukla, N., Berardi, U., El-Korchi, T., and Dessel, S. V., "Design and Application of Concrete Tiles Enhanced with Microencapsulated Phase-Change Material," *Journal of Architectural Engineering*, Vol. 22, 2016.

[43] *Annual Book of ASTM Standards*, Vol. 04.02, ASTM.

[44] "Emissivity in the Infrared," OptoTherm, Inc., https://www.optotherm.com/emiss-table.htm, 2018.

[45] Wilson, J., "Thermal Properties of Building Materials," February 2008.

[46] "Polyethylene - Low Density (LDPE)," Goodfellow, http://www.goodfellow.com/E/Polyethylene-Low-Density.html.

[47] "Rigid Fiberglass Duct Insulation Sheets," McMaster-Carr, https://www.mcmaster.com/thermal-insulation.

[48] "Insulation," U.S. Department of Energy, https://www.energy.gov/energysaver/weatherize/insulation.

[49] Howlader, M. K., Rashid, M. H., Mallick, D., and Haque, T., "Effects of Aggregate Types on Thermal Properties of Concrete," *ARPN Journal of Engineering and Applied Sciences*, Vol. 7, No. 7, July 2012.

[50] Chen, J., Chu, R., Wang, H., and Xie, P., "Experimental Measurement and Microstructure-Based Simulation of Thermal Conductivity of Unbound Aggregates," *Construction and Building Materials*, Vol. 189, 2018.

[51] Kenisarin, M., Mahkamov, K., Kahwash, F., and Makhkamova, I., "Enhancing thermal condutivity of paraffin wax 53-57 ° C using expanded graphite," *Solar Energy Materials and Solar Cells*, Vol. 200, No. 110026, September 2019.

[52] Malik, A., Ogden, S., Amberg, G., and Hjort, K., "Modeling and Analysis of a Phase Change Material Thermohydraulic Membrane Microactuator," *Journal of Microelectromechanical Systems*, 2012.

[53] Incopera, F. P., DeWitt, D. P., Bergman, T. L., and Lavine, A. S., *Fundamentals of Heat and Mass Transfer, 6th Edition*, John Wiley & Sons, 2007.

APPENDICES

APPENDIX A

Python Code for Convection Coefficient

A.1 Convection Calculation

This is the code used to calculate convection coefficients

```
#ConvectionCalc.py
#Horizontal Plate Convection calculation for obtaining
#temperature dependent convection coefficient.
import matplotlib.pyplot as plt
import numpy as np
from scipy.constants import g
Lcpad = .4064#meters or 4/3 ft
Lcside = .3048#meters or 1 ft. All sides the same since they're just as tall.
#Horizontal flat plate (top of heated or bottom of cooled) Nusselt number
def nusselt(Ra):
    """Nusselt number for upper surface of heated horizontal flat plate"""
    if Ra < 10**2:
        print("Rayleigh number too low")
        return 1
    elif Ra > 10**11:
        print("Rayleigh number too high")
    else:
        if Ra < 10**7:
            return .9*Ra**.23
        else:
            return .15*Ra**(1/3)

def nusseltlow(Ra):
    """Nusselt number for lower surface of horizontal hot plate or
    upper surface of cold plate"""
    if Ra < 10**5:
        print("Rayleigh number too low")
        return 1
    elif Ra > 10**10:
        print("Rayleigh number too high")
        return 1
    else:
        return .27*Ra**(1/4)
#Air property lists:
Ta = [250,300,350,400,450,500]
rhoa = [1.3947,1.1614,.9950,.8711,.774,.6964]
va = [11.44e-6,15.89e-6,20.92e-6,26.41e-6,32.39e-6,38.79e-6]
ala = [15.9e-6,22.5e-6,29.9e-6,38.3e-6,47.2e-6,56.7e-6]
Pra = [.72,.707,.7,.69,.686,.684]
ka = [22.3e-3,26.3e-3,29.9e-3,30e-3,33.8e-3,37.3e-3]
def interp(data,T):
    if T < Ta[0]:
        print("Need more data - too low")
        return 1
    elif T > Ta[-1]:
        print("Need more data - too high")
        return 1
    else:
        i = 0
        while Ta[i+1] < T:
            i+=1
        return data[i]+(T-Ta[i])*(data[i+1]-data[i])/(Ta[i+1]-Ta[i])
def Rayleigh(Ts,Tinf,Lc):
```

```
    Tf = (Ts+Tinf)/2
    return g*(Ts-Tinf)*Lc**3/(interp(va,Tf)*interp(ala,Tf)*Tf)
def hcoef(Ts,Tinf,Lc):
    Tf = (Ts+Tinf)/2
    return nusselt(Rayleigh(Ts,Tinf,Lc))*interp(ka,Tf)/Lc
def hcoeflow(Ts,Tinf,Lc):
    Tf = (Ts+Tinf)/2
    return nusseltlow(Rayleigh(Ts,Tinf,Lc))*interp(ka,Tf)/Lc
def hcoefvert(Ts,Tinf,L):
    Tf = (Ts+Tinf)/2
    return (interp(ka,Tf)/L)*(.825+.387*Rayleigh(Ts,Tinf,L)**(1/6)/\
    (1+(.492/interp(Pra,Tf))**(9/16))**(8/27))**2
```

A.2 Exporting Script

Code for exporting coefficient values to be imported to ANSYS

```
xml1 = '''<?xml version="1.0" encoding="UTF-8" standalone="no" ?>
<ANSYS_EnggData>
    <MaterialData/>
    <ConvectionData/>
    <LoadVariationData>
          <MatML_Doc>
              <LoadVariation>
                    <BulkDetails>
                        <Name>'''
xml1a= '''</Name>
                        <Form>
                              <Description/>
                    </Form>
                        <PropertyData property="pr1">
                              <Data format="float">'''
xml2 = '''</Data>
                              <Qualifier>Temperature</Qualifier>
                              <ParameterValue format="float" parameter="pa1">'''
xml3 = '''</ParameterValue>
                    </PropertyData>
                </BulkDetails>
                    <Metadata>
                        <ParameterDetails id="pa1">
                              <Name>Time</Name>
                    </ParameterDetails>
                        <PropertyDetails id="pr1">
                              <Name>Temperature</Name>
                    </PropertyDetails>
                </Metadata>
            </LoadVariation>
        </MatML_Doc>
    </LoadVariationData>
    <BeamSectionData/>
</ANSYS_EnggData>
'''
xmlc1 = '''<?xml version="1.0" encoding="UTF-8" standalone="no" ?>
<ANSYS_EnggData>
    <MaterialData/>
    <ConvectionData/>
    <LoadVariationData>
          <MatML_Doc>
              <LoadVariation>
                    <BulkDetails>
                        <Name>'''
xmlc2 = '''</Name>
                        <Form>
                              <Description></Description>
                    </Form>
                        <PropertyData property="pr1" technique="mt1">
                              <Data format="float">'''
```

```
xmlc3 = '''</Data>
                            <Qualifier>Convection Coefficient</Qualifier>
                            <ParameterValue format="float" parameter="pa1">'''
xmlc4 = '''</ParameterValue>
                        </PropertyData>
                    </BulkDetails>
                        <Metadata>
                            <MeasurementTechniqueDetails id="mt1">
                                <Name>Difference of Surface and Bulk Temp</Name>
                        </MeasurementTechniqueDetails>
                            <ParameterDetails id="pa1">
                                <Name>Temperature</Name>
                        </ParameterDetails>
                            <PropertyDetails id="pr1">
                                <Name>Convection Coefficient</Name>
                            </PropertyDetails>
                    </Metadata>
                </LoadVariation>
            </MatML_Doc>
    </LoadVariationData>
    <BeamSectionData/>
</ANSYS_EnggData>'''
def ansysout(name,temps,times):
    '''temps and times should be lists, name should be a string'''
    with open('c:/Users/MTL/Documents/'+name+'.xml',mode='w') as output:
        output.write(xml1)
        output.write(name)
        output.write(xml1a)
        for item in temps:
            output.write(str(round(item,2))+',')
        else:
            pos = output.tell()
            output.seek(pos-1,0)
        output.write(xml2)
        for item in times:
            output.write(str(round(item,2))+',')
        else:
            pos = output.tell()
            output.seek(pos-1,0)
        output.write(xml3)

def ansysconv(name,temps,coefs):
    '''temps and coefs should be lists, name should be a string'''
    with open('c:/users/MTL/Documents/'+name+'.xml',mode='w') as output:
        output.write(xmlc1)
        output.write(name)
        output.write(xmlc2)
        for item in coefs:
            output.write(str(round(item,2))+',')
        else:
            pos=output.tell()
            output.seek(pos-1,0)
        output.write(xmlc3)
        for item in temps:
            output.write(str(round(item,2))+',')
        else:
            pos = output.tell()
            output.seek(pos-1,0)
        output.write(xmlc4)
```